Intrinsic Kinetics of the Internal Steam Reforming of CH4 over a Ni−YSZ−Cermet Catalyst−Electrode

ARTICLE *in* INDUSTRIAL & ENGINEERING CHEMISTRY RESEARCH · OCTOBER 2000

Impact Factor: 2.59 · DOI: 10.1021/ie000350u

Intrinsic Kinetics of the Internal Steam Reforming of CH_4 over a Ni−YSZ−Cermet Catalyst−Electrode

Simeon Bebelis,[†] Andonis Zeritis,[†] Constantina Tiropani,[†] and Stylianos G. Neophytides*[,‡]

Department of Chemical Engineering, University of Patras, GR-26500 Patras, Greece, and Institute of Chemical Engineering and High Temperature Chemical Processes, P.O. Box 1414, GR-26500 Patras, Greece

The kinetics of steam reforming of methane were studied on a Ni−$ZrO_2(Y_2O_3)$−cermet film, at temperatures of 1073−1173 K and methane and steam partial pressures of up to 60 and 5 kPa, respectively. It was found that the reaction exhibits Langmuir−Hinselwood kinetic behavior, corresponding to competitive adsorption of methane (in the form of active carbon species, C_{ad}) and H_2O (in the form of adsorbed oxygen species, O_{ad}) on the catalytic surface. Kinetic results concerning methane consumption were explained in the frame of a mechanistic scheme involving two rate-limiting steps. These steps correspond (i) to the activated adsorption of CH_4 for the production of active carbon species, C_{ad}, and (ii) to the surface reaction of the adsorbed C_{ad} with the O_{ad} species, originating from the adsorption of H_2O, for the production of CO. The relative magnitude of the turnover frequencies of these two rate-limiting steps affects considerably the apparent activation energy of the reaction at different P_{CH_4} and P_{H_2O} values as well as the tendency of the reaction system to generate graphitic carbon on the catalytic surface. Regarding CO_2 formation rate, the kinetic results were explained by considering as the rate-determining step the surface reaction of the adsorbed CO_{ad} with adsorbed oxygen species.

Introduction

One of the key aspects for the efficient operation of solid oxide fuel cells (SOFCs) is the suitable choice of fuel. The most frequently used fuel is H_2, which is mainly produced by steam reforming of CH_4 on Ni-based catalysts at temperatures ranging from 973 to 1173 K.[1] However, CH_4 or natural gas can also be directly introduced to SOFCs as fuels without the need of an external reformer. This is due to the catalytic action for steam reforming of methane of the fuel-exposed Ni surface of the state-of-the-art Ni−$ZrO_2(Y_2O_3)$ (or Ni−YSZ)−cermet anode, in the temperature range of SOFC operation.

According to this process, which is known in the literature as internal steam reforming of methane (ISRM), the Ni surface of the Ni−YSZ−cermet anode catalyzes the steam reforming reaction of CH_4 (reaction 1) as well as the water−gas shift reaction (reaction 2):

$$CH_4 + H_2O \rightarrow CO + 3H_2 \quad (1)$$

$$CO + H_2O \rightarrow CO_2 + H_2 \quad (2)$$

thus producing H_2, CO, and CO_2. The produced hydrogen and carbon monoxide can then be readily oxidized electrochemically at the three phase boundaries (Ni|YSZ|gas), generating electricity:

$$H_2 + O^{2-} \rightarrow H_2O + 2e^- \quad (3)$$

$$CO + O^{2-} \rightarrow CO_2 + 2e^- \quad (4)$$

The simulation and design of a SOFC requires information on thermodynamics and kinetics of reactions 1−4. Thermodynamics are fairly well accounted for, while there is severe lack of information regarding kinetics of reactions 1−4. Considerable attention was paid in the past concerning the preparation of the Ni−YSZ−cermet anodes and the evaluation of the process and equipment, while the limited number of kinetic investigations was based on power law kinetics and/or corresponded to a restricted range of reaction conditions.[2−8] In this respect, the proposed rate equations are of limited importance for the simulation, design, and scale-up of SOFCs.

The kinetic behavior of the methane steam reforming reaction over Ni-supported industrial catalysts has been given considerable attention by many researchers and a very large number of relevant studies have been published.[1,9−18] Despite the considerable effort, no agreement has yet been established concerning the main catalytic steps that determine reaction rate behavior. Discrepancies and contradictions still exist, concerning the effective reaction order with respect to both steam and CH_4. Xu and Froment[16] proposed a general rate equation based on several surface reaction steps, according to the Langmuir−Hinshelwood−Hougen−Watson (LHHW) model, which describes the intrinsic kinetics of the reaction on a Ni−$MgAl_2O_3$−spinel catalyst.

The present paper deals with the detailed description of the CH_4 steam reforming reaction kinetics on Ni−YSZ−cermet catalyst−electrodes under open-circuit conditions. A kinetic expression is derived describing quantitatively the basic surface reactions on the Ni−YSZ−cermet surface, which result in transformation of CH_4 to H_2, CO, and CO_2.

Experimental Section

The atmospheric pressure continuous flow apparatus has been described previously.[5,7,8] Helium was saturated

* To whom correspondence should be addressed.
[†] University of Patras.
[‡] Institute of Chemical Engineering and High Temperature Chemical Processes.

10.1021/ie000350u CCC: $19.00
Published on Web 10/28/2000

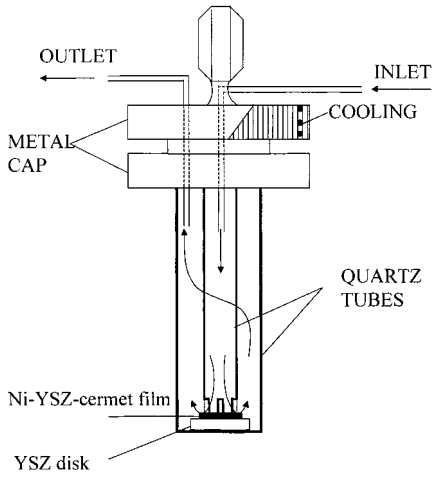

Figure 1. Reactor cell configuration.

with water by sparging it through a thermostated water saturator and was subsequently mixed with a CH_4/He mixture. The reactor inlet steam concentration was controlled by varying both the saturator temperature and the He flow. CH_4-certified standard and ultrapure 99.999% He (L'Air Liquide) were used. Reactants and products were analyzed by online gas chromatography using a Shimadzu 14A gas chromatograph with a thermal conductivity detector. The chromatograms were integrated and analyzed using a Shimadzu C-R5A integrator. A Porapak QS column (80/100 mesh, 8 ft length $\times$ $^1/_8$ in. o.d.) was used for H_2O analysis at 393 K, while a Carbosieve column (80/100 mesh, 8 ft length $\times$ $^1/_8$ in. o.d.) was used for the separation of H_2, CO, CH_4, and CO_2 at 453 K. Although He was the carrier gas, H_2 could be detected and measured because of the small volume of the injected reaction mixture. All lines and valves were heated at 423 K to prevent water condensation.

The atmospheric pressure continuous flow reactor had a volume of 30 cm^3 and was made of a quartz tube closed at one end (Figure 1). The open end of the tube was mounted on a stainless steel cap, which had provisions for the introduction of reactants and removal of products. The Ni−YSZ catalyst−electrode was deposited on a YSZ disk (2 cm diameter and 2 mm thickness) in the form of a porous film of a geometric area of ~0.1 cm^2. The YSZ disk was clamped inside the reactor between two quartz tubes, as shown in Figure 1.

The porous Ni−YSZ−cermet anode contained 70 wt % Ni and was produced via a slurry technique,[3,5] starting from $Ni(NO_3)_2$ and Zircar YSZ powder (ZYP; 8 mol % Y_2O_3, BET area = 14 m^2/g). Preweighed amounts of YSZ powder and an aqueous $Ni(NO_3)_2$ solution were mixed, magnetically stirred, and mildly heated to 573 K. The resulting green precipitate was then heated at 873 K to decompose the nitric salt to NiO. The product was subsequently milled in *n*-butyl acetate for 2 h, dried overnight, and blended with a small (2 wt %) amount of a poly(vinyl alcohol) binder solution. A thin coating of the resulting paste was deposited on a YSZ disk and calcinated in air at 1773 K for 1 h, followed by reduction in H_2/He (5/95 vol %) flow for 2 h. The resistance across the resulting Ni−YSZ−cermet film was less than 1 Ω even at room temperature. The amount of the deposited Ni−YSZ−cermet on the YSZ disk was 3 mg, and the Ni true surface area was equal to 25 cm^2, corresponding to a very low (1.2×10^{-3}) Ni dispersion, due to the high Ni content of the Ni−YSZ−cermet. The measurement of the Ni true surface area was performed in a static volumetric apparatus (Accusorb 2100E, Micromeritics) using H_2 chemisorption at room temperature. The sample used in these measurements was 1 g of Ni−YSZ powder, taken from the same batch and sintered at the same temperature (1773 K) as the amount of the 3 mg deposited on the YSZ disk.

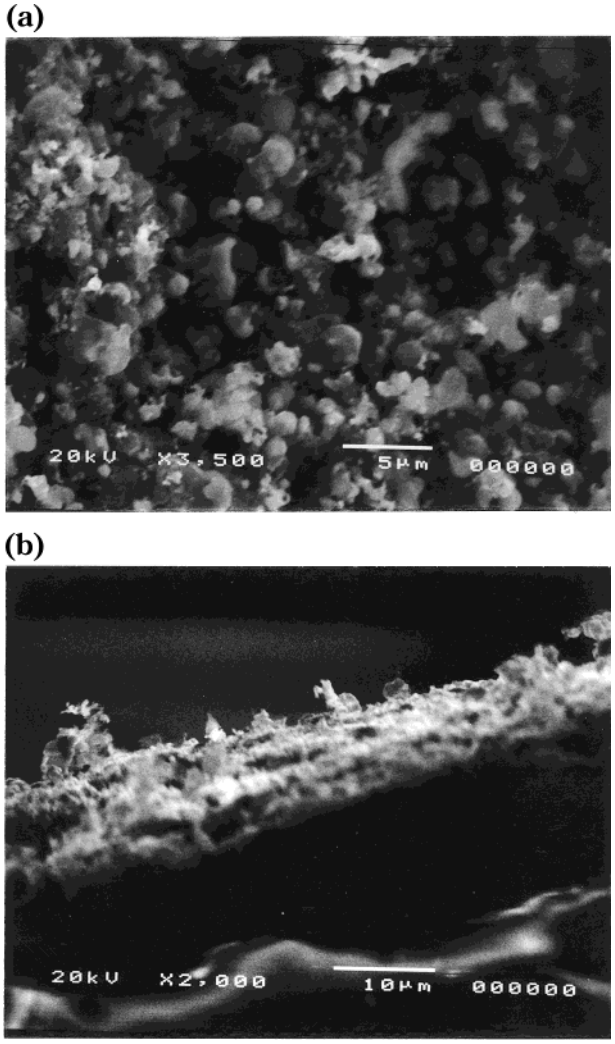

Figure 2. Scanning electron micrographs of the top side of the Ni−YSZ catalyst (a) and of a cross section perpendicular to the Ni−YSZ catalyst|YSZ disk interface (b).

Figure 2 shows scanning electron micrographs of the top side of the Ni−YSZ catalyst film (Figure 2a) and of a cross section perpendicular to the Ni−YSZ catalyst|YSZ interface (Figure 2b). The micrograph of the top side (Figure 2a) shows a porous electrode with the size of particles on the order of 1 μm, while the micrograph of the cross section (Figure 2b) shows that the thickness of the catalyst−electrode film is on the order of 10 μm, allowing one to safely consider the internal diffusion resistance of the porous film to be negligible. The composition of the catalyst surface was determined using X-ray photoelectron spectroscopy (XPS) and was found to be equal to 75 wt % Ni, very close to the bulk chemical composition of Ni−YSZ−cermet (70 wt % Ni) corresponding to the preparation procedure. This result strongly indicates that there is a weak interaction between Ni and YSZ (i.e., YSZ is not covered by Ni) and that the two phases are completely segregated, thus forming a homogeneous mixture of Ni and yttria-stabilized zirconia particles. This conclusion is corroborated by the results of Sotiropoulou and Ladas,[19]

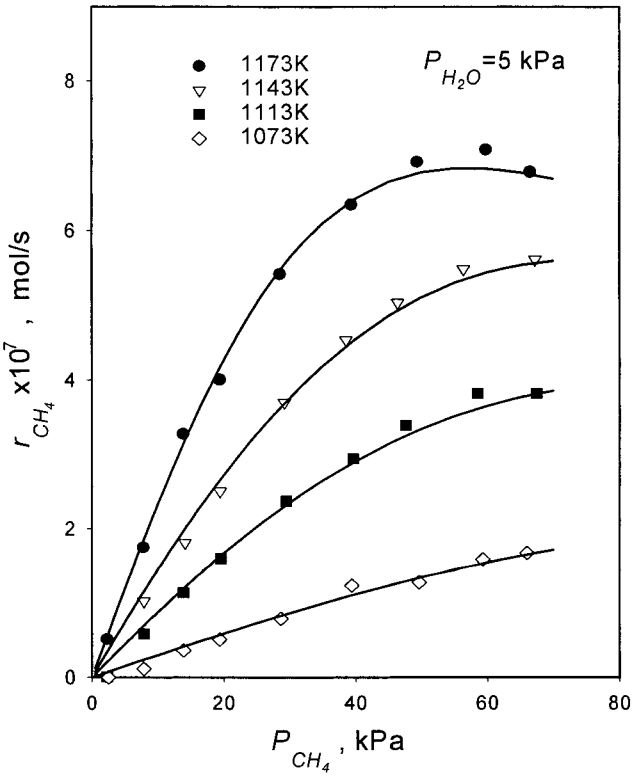

Figure 3. Kinetic effect of P_{CH_4} on the CH_4 consumption rate, r_{CH_4}, at various temperatures and $P_{H_2O} = 5$ kPa. The solid curves correspond to the predictions of the kinetic model (eq 13).

who investigated the interface formation of Ni and YSZ and found that there is a very weak interaction between YSZ and Ni resulting in a small amount of electronic transfer, probably because of the interaction of Ni atoms with the O^{2-} of the YSZ surface.

Within the flow rate used in this investigation, i.e., between 440 and 500 mL STP/min (equivalently, between 3.3×10^{-4} and 3.7×10^{-4} mol/s), the reactor was operating under differential conditions, with reactant conversion being lower than 4%, and was found to exhibit CSTR (continuous stirred tank reactor) behavior. The absence of external mass-transfer limitations and reaction thermodynamic equilibrium constraints was also checked. The reaction rate of CO and CO_2 formation was found to remain practically constant for total flow rates varying from 1.4×10^{-4} to 3.7×10^{-4} mol/s. No changes in the activity of the Ni−YSZ−cermet catalyst were observed throughout the kinetic experiments, thus excluding the possibility of catalyst deactivation due to carbon deposition.

Results

The dependence of the reaction rate on the partial pressure of methane, P_{CH_4}, and steam, P_{H_2O}, measured at the reactor exit, was studied at four different temperatures varying between 1073 and 1173 K. At each temperature the kinetic effect of P_{CH_4} was examined at four different P_{H_2O}. The partial pressures of CH_4 and H_2O were varied between 0.5 and 80 kPa and 0.5 and 5 kPa, respectively, while the total pressure was atmospheric. Helium was used as a diluent, so that CH_4 or H_2O partial pressures in the reactor could be varied while keeping one of them constant.

Figures 3−5 depict the kinetic behavior of the intrinsic catalytic reaction rate of the steam reforming of CH_4. The effect of P_{CH_4} on the consumption rate of methane,

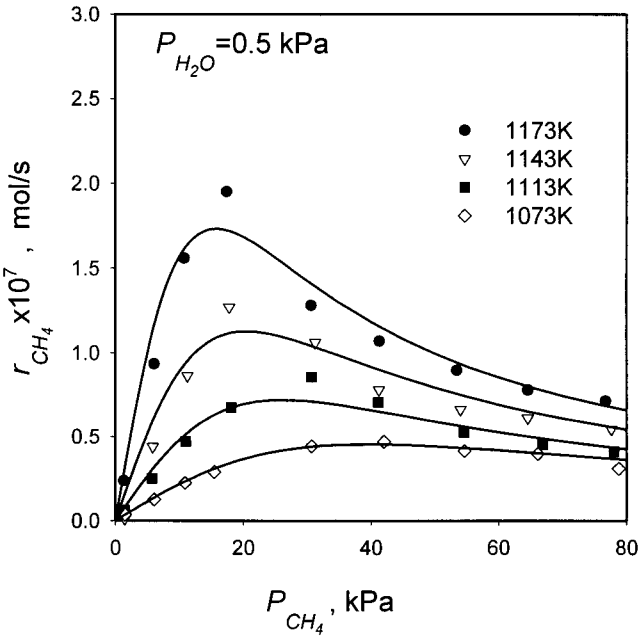

Figure 4. Kinetic effect of P_{CH_4} on the CH_4 consumption rate, r_{CH_4}, at various temperatures and $P_{H_2O} = 0.5$ kPa. The solid curves correspond to the predictions of the kinetic model (eq 13).

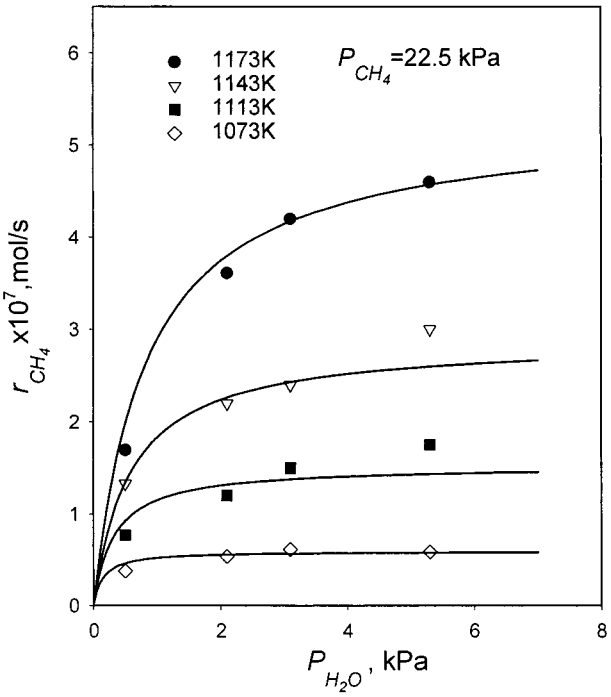

Figure 5. Kinetic effect of P_{H_2O} on the CH_4 consumption rate, r_{CH_4}, at various temperatures and $P_{CH_4} = 22.5$ kPa. The solid curves correspond to the predictions of the kinetic model (eq 13).

with the latter being equal to the sum of CO and CO_2 formation rates, at various temperatures and constant P_{H_2O}, is shown in Figures 3 and 4, for P_{H_2O} equal to 5 and 0.5 kPa, respectively. As shown in these figures, more clearly in Figure 3, the reaction rate increases almost linearly, with increasing P_{CH_4}, for low P_{CH_4} values and up to a ratio of $P_{CH_4}/P_{H_2O} \cong 5$. When P_{CH_4} is further increased, the reaction rate reaches a maximum value, while at even higher P_{CH_4} values, the rate decreases, exhibiting negative order kinetics with respect to CH_4. This behavior is more evident at lower H_2O partial pressures (Figure 4). The existence of a maximum in the reaction rate implies that methane and water are

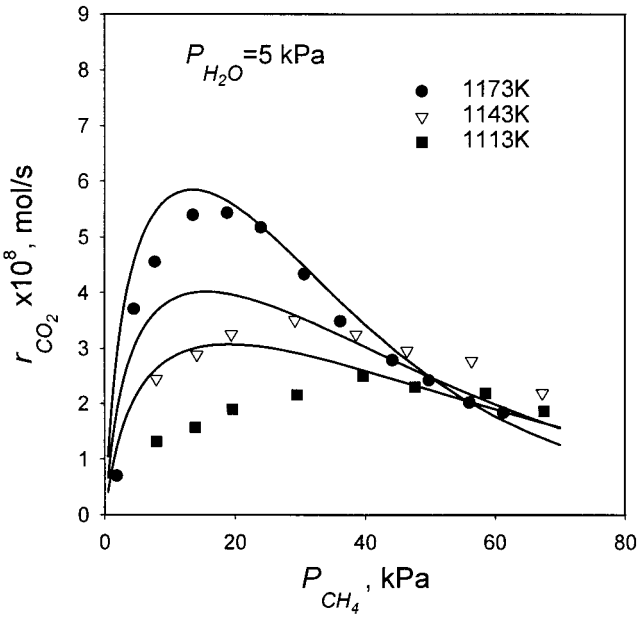

Figure 6. Effect of P_{CH_4} on the rate of CO_2 formation, r_{CO_2}, at various temperatures and P_{H_2O} = 5 kPa. The solid curves correspond to the predictions of the kinetic model (eq 18).

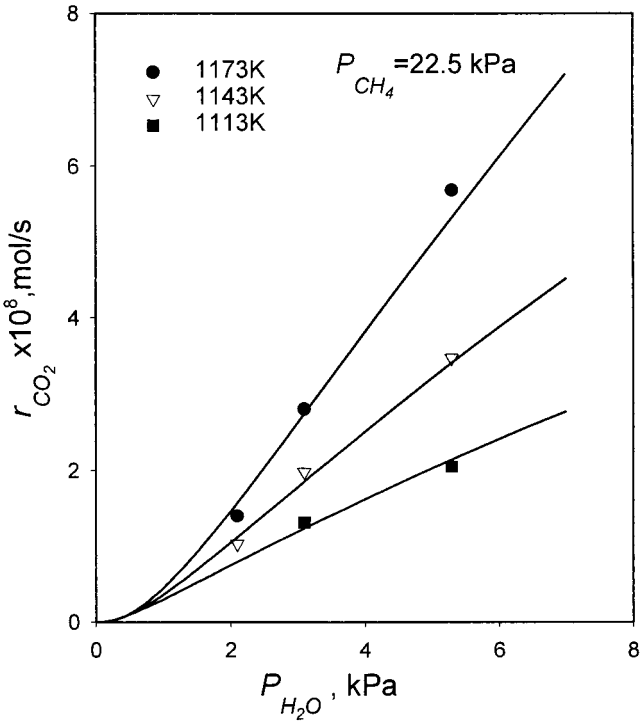

Figure 7. Effect of P_{H_2O} on the rate of CO_2 formation, r_{CO_2}, at various temperatures and P_{CH_4} = 22.5 kPa. The solid curves correspond to the predictions of the kinetic model (eq 18).

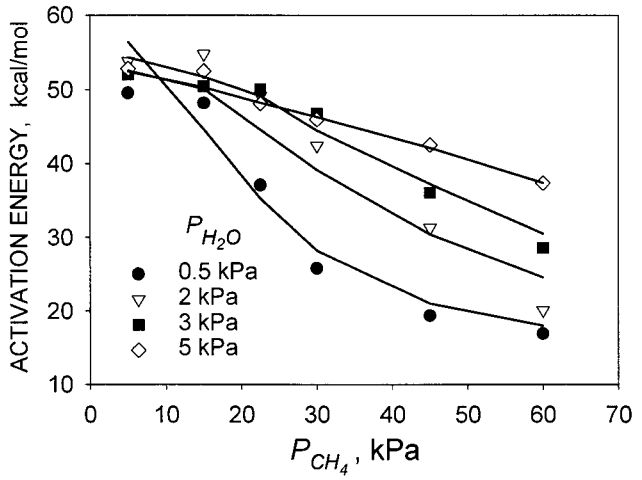

Figure 8. Effect of P_{CH_4} on the apparent activation energy of the methane reforming reaction at various P_{H_2O} values. The solid curves correspond to the predictions of the kinetic model (eq 13).

competitively adsorbed on the Ni surface and that their kinetics can be described within the general framework of the classical Langmuir−Hinshelwood kinetic model. It is worth noticing that with increasing temperature there is a gradual shift of the rate maximum location toward lower P_{CH_4} values. As will be discussed, such behavior strongly indicates that the dissociative adsorption of CH_4 (most probably in the form of active carbon[20]) proceeds faster at higher temperatures. Thus, a lower P_{CH_4} value is needed so that the coverage of the resulting adsorbed species can reach the value corresponding to the maximum of the reaction rate.

The effect of P_{H_2O} on the reaction rate, at constant P_{CH_4} = 22.5 kPa, is shown in Figure 5. The reaction rate exhibits a Langmuir type kinetic behavior, approximating zero-order dependence at high P_{H_2O}. As will be further discussed in detail, this kinetic behavior corroborates the conclusion that the coverage of the adsorbed species resulting from the dissociative adsorption of H_2O on the Ni surface (e.g., O_{ad}) can be significantly low even at high P_{H_2O}.

The effect of varying P_{CH_4} and P_{H_2O} on the rate of CO_2 formation is depicted in Figures 6 and 7. As shown in Figure 6, a maximum in the CO_2 formation rate, r_{CO_2}, appears with increasing P_{CH_4}, at significantly lower P_{CH_4} values, compared to the ones corresponding to the maximum of the CH_4 consumption rate (Figure 3). The maximum in r_{CO_2} is also slightly shifted toward lower P_{CH_4} with increasing reaction temperature. Assuming that CO_2 is formed by sequential oxidation of CO_{ad}, the appearance of the r_{CO_2} maximum at lower P_{CH_4} values indicates that CO_{ad} species are readily displaced by the species resulting from the dissociative adsorption of methane. As shown in Figure 7, at constant P_{CH_4} = 22.5 kPa, the rate of CO_2 formation seems to vary almost linearly with P_{H_2O} for P_{H_2O} > 2 kPa. The selectivity to CO_2 approaches a value of 30% at P_{CH_4}/P_{H_2O} ratios typically on the order of 0.5, while it is dramatically decreased at higher P_{CH_4} values.

Figure 8 shows the effect of varying P_{CH_4} on the apparent activation energy of the methane reforming reaction at various P_{H_2O} values. For all P_{H_2O} values, the apparent activation energy decreases with increasing P_{CH_4}. At low P_{CH_4} values, the apparent activation energy is approximately equal to 50 kcal/mol, being, within experimental error, the same for all water partial pressures shown in Figure 8. On the contrary, for P_{CH_4} higher than approximately 20 kPa, the apparent activation energy is progressively decreasing with increasing P_{H_2O}, reaching its lowest value (equal to 19 kcal/mol) at P_{H_2O} = 0.5 kPa.

Discussion

Model Development. Reaction Schemes. One of the key aspects in deriving a reliable mechanistic model is the proper determination of the rate-limiting step. As has already been mentioned above, the gradual shift of the location of the methane consumption rate maximum

toward lower P_{CH_4} values can be attributed to the kinetic effect of temperature on the adsorption rate of CH_4 on the catalytic surface. The dissociative adsorption rate of CH_4 on the Ni surface increases with increasing temperature, and according to the Langmuir−Hinshelwood kinetic model, such behavior is expected to result in the appearance of the rate maximum location at lower P_{CH_4} values. This is due to the attained higher coverage of the generated adsorbed species at even lower P_{CH_4} values. The above considerations lead to the conclusion that the dissociative adsorption of CH_4 on the Ni surface is an activated process and can be considered as a rate-limiting step in the catalytic mechanism of the CH_4 steam reforming reaction. This is a conclusion supported by a large number of researchers in the past.[21−27] A significant number of both experimental and theoretical work has been devoted to the understanding of the dissociative chemisorption of methane on Ni surfaces.[21−27] Both thermal desorption and kinetic studies[21]and molecular beam experiments[22,24] have been used to probe the nature of "C−H bond activation" on Ni, as well as on other metal surfaces.[25] The activation energies, determined from thermal adsorption and molecular beam experiments for the methane dissociative adsorption on Ni, range between 12 and 22 kcal/mol,[21,22,24] while activation energies as high as 24 kcal/mol were estimated based on theoretical model calculations.[23,26,27]

As is generally accepted in the literature,[16] H_2O is dissociatively adsorbed on the surface Ni atoms, producing adsorbed oxygen, O_{ad}, and gaseous H_2 which are in thermodynamic equilibrium, as described by the overall surface reaction:

$$H_2O + S \leftrightarrow O_{ad} + H_2(g) \tag{5}$$

Although the formation of hydroxyl species, instead of O_{ad}, cannot be excluded, dissociation of H_2O according to eq 5 was assumed because it resulted in the most adequate fitting of the kinetic data. With increasing reaction temperatures (Figure 5), the observed plateau in the reaction rate is reached at higher P_{H_2O} values, strongly indicating, according to Langmuir kinetic considerations, that the dissociative adsorption of the H_2O molecule on the Ni surface (eq 5) is an equilibrium adsorption process, which can be described by

$$K_{H_2O} = \frac{\theta_O P_{H_2}}{\theta_s P_{H_2O}} \tag{6}$$

where θ_O and θ_s are the coverages corresponding to the adsorbed oxygen and the empty sides, respectively. Because the adsorption equilibrium constant K_{H_2O} is a decreasing function of temperature, the coverage θ_O of O_{ad} on Ni is expected to decrease with increasing temperature, while maintaining P_{H_2}/P_{H_2O} constant. When P_{H_2O} is adjusted at a higher value, a higher O_{ad} coverage is formed on the catalytic surface, thus compensating the effect of the increase in reaction temperature.

Furthermore, the zero-order dependence of the methane consumption reaction rate on P_{H_2O} at high P_{H_2O} is a good indication that O_{ad} is weakly adsorbed on the Ni surface. Because CH_4 and H_2O are competitively adsorbed on the catalytic surface, the constancy of the reaction rate at high P_{H_2O} values indicates that O_{ad} coverage is very low, so that it does not affect significantly either the concentration of the vacant sites or the coverage of the species originating from CH_4 adsorption.

Although CH_4 adsorption, resulting in chemisorbed carbon species C_{ad} and gaseous H_2, is a multistep surface reaction,[16] it can be represented by the overall surface reaction

$$CH_4 + S \rightarrow C_{ad} + 2H_2(g) \tag{7}$$

Thus, the CH_4 consumption rate is given by

$$r_{CH_4} = k_{ad} P_{CH_4} \theta_s \tag{8}$$

where k_{ad} denotes the kinetic constant for methane dissociative adsorption. If the O_{ad} coverage is very low and thus θ_s is essentially constant, then it is clear from eq 8 that r_{CH_4} will be zero order with respect to P_{H_2O} at constant P_{CH_4}. However, if CH_4 adsorption (eq 7) was the only rate-determining step, r_{CH_4} would have been independent of P_{H_2O} even at very low P_{H_2O} values. On the contrary, starting from low P_{H_2O}, the reaction rate is progressively increasing with increasing P_{H_2O} and approaches a maximum constant value at higher P_{H_2O} values. Such behavior can be explained only by consideration of an additional rate-determining step, involving the surface reaction of C_{ad} with O_{ad}:

$$C_{ad} + O_{ad} \rightarrow CO_{ad} + S, \quad r_{CH_4} = k_r \theta_c \theta_O \tag{9}$$

where θ_c is the coverage of C_{ad}.

This is also corroborated by the observed maximum in the reaction rate (Figures 3 and 4) and the significant decrease in the apparent activation energy with increasing P_{CH_4} (Figure 8).

Kinetic Expression for the Methane Reforming Rate. Considering the rate-determining reaction steps described by eqs 7 and 9 and the equilibrium reaction 5 and assuming that CO_{ad} coverage, θ_{CO}, and θ_O are very small, the rate of methane consumption r_{CH_4} is given by

$$r_{CH_4} = k_{ad} P_{CH_4} \left(1 - \frac{k_{ad}}{k_r K_{H_2O}} \frac{P_{H_2} P_{CH_4}}{P_{H_2O}}\right) \tag{10}$$

Under steady-state conditions, the combination of C, O, and H mass balances, according to the stoichiometries of the reforming (eq 1) and water−gas shift (eq 2) reactions, results in the following equality:

$$r_{H_2} = 3r_{CO} + 4r_{CO_2} = 3r_{CH_4} + r_{CO_2} \tag{11}$$

where the rate of carbon deposition is assumed to be negligible. This assumption is based on the experimental evidence, according to which eq 11 is experimentally valid within 1−2%.

Because $r_{H_2} = (P_{H_2})/(P_t)F_t$, where F_t is the total molar flow rate at the reactor outlet, eq 11 can be written as

$$P_{H_2} = \frac{3r_{CH_4} + r_{CO_2}}{F_t} P_t \tag{12}$$

where $P_t = 100$ kPa is the total pressure in the reactor.

Substitution of eq 12 into eq 10 results in

$$r_{CH_4} = \frac{k_{ad} P_{CH_4} P_{H_2O} F_t - k P_{CH_4}{}^2 r_{CO_2}}{P_{H_2O} F_t + 3k P_{CH_4}{}^2} \tag{13}$$

where

$$k = \frac{k_{ad}^{\ 2}}{K_{H_2O} k_r} \tag{14}$$

Equation 13 describes the effect of P_{CH_4} and P_{H_2O} on the rate of CH_4 consumption. As can be derived from model eq 13, $r_{CH_4} \cong k_{ad} P_{CH_4}$ at low P_{CH_4} values, which exemplifies the dominant role of CH_4 adsorption.

Kinetic Expression for the CO_2 Formation Rate. As has already been mentioned in the discussion of Figure 6, CO_2 formation is considered to involve the surface reaction of adsorbed CO_{ad} with O_{ad}:

$$CO_{ad} + O_{ad} \rightarrow CO_2 + 2S, \quad r_{CO_2} = k_{CO_2} \theta_{CO} \theta_O \tag{15}$$

while adsorbed CO_{ad} is assumed to be in equilibrium with CO in the gas phase:

$$CO + S \leftrightarrow CO_{ad}, \quad K_{CO} = \frac{\theta_{CO}}{P_{CO} \theta_s} \tag{16}$$

By combining eqs 8, 13, 15, and 16, while assuming that $r_{CO_2} \ll 3 r_{CH_4}$ (as experimentally observed) and taking into account that

$$P_{CO} = \frac{r_{CH_4} - r_{CO_2}}{F_t} P_t \tag{17}$$

the following equation results, which describes the effect of P_{CH_4} and P_{H_2O} on the rate of CO_2 formation:

$$r_{CO_2} = \frac{k_w r_{CH_4}^{\ 2} P_{H_2O}}{k_{ad}^{\ 2} P_{CH_4}^{\ 2} + k_w r_{CH_4} P_{H_2O}} \tag{18}$$

where

$$k_w = k_{CO_2} K_{CO} K_{H_2O} \tag{19}$$

Estimation of the Parameters of the Kinetic Model. The kinetic expressions corresponding to eqs 13 and 18 can be fitted to the experimental data quite well, as shown by the solid lines in Figures 3−8. The resulting values of the kinetic constants k_{ad}, k, and k_w satisfy the Arrhenius equation (Figure 9). The corresponding activation energies and the mean values of these parameters at the temperatures of the present study are shown in Table 1.

The temperature dependence of the adsorption rate constant of CH_4, k_{ad}, is given by

$$k_{ad} = k_{ad}^{o} \exp\left(-\frac{27531 \pm 1100}{T}\right) \tag{20}$$

The activation energy corresponding to k_{ad} is equal to 54.7 ± 2.2 kcal/mol, which is close to the upper limit of the apparent activation energies (17−71 kcal/mol) so far reported in the literature,[1,3−18] under conditions where the reaction rate varies linearly with varying P_{CH_4}. Xu and Froment[16] and Castro Luna and Becerra[18] reported activation energies for the steam reforming reaction as high as 57.6 kcal/mol in the case of the Ni−$MgAl_2O_4$ catalyst and 71 kcal/mol in the case of a Ni−alumina−titania catalyst, respectively. According to the kinetic model proposed by Xu and Froment,[16] the apparent activation energy could not be lower than the positive enthalpy change of the reforming reaction. They also attributed to diffusional limitations or nonisothermal operation the fact that the majority of the authors who used porous catalysts obtained very low activation energies compared to the ones reported in their work.[16] Lee et al.[3] reported activation energies ranging between 17.8 and 23.5 kcal/mol for Ni−YSZ−cermet powder, while Belyaev et al.[4] calculated a value of 39 kcal/mol for a Ni−ZrO_2−CeO_2 electrode−catalyst. A recent study on Ni−YSZ−cermet anodes[7] reports activation energies

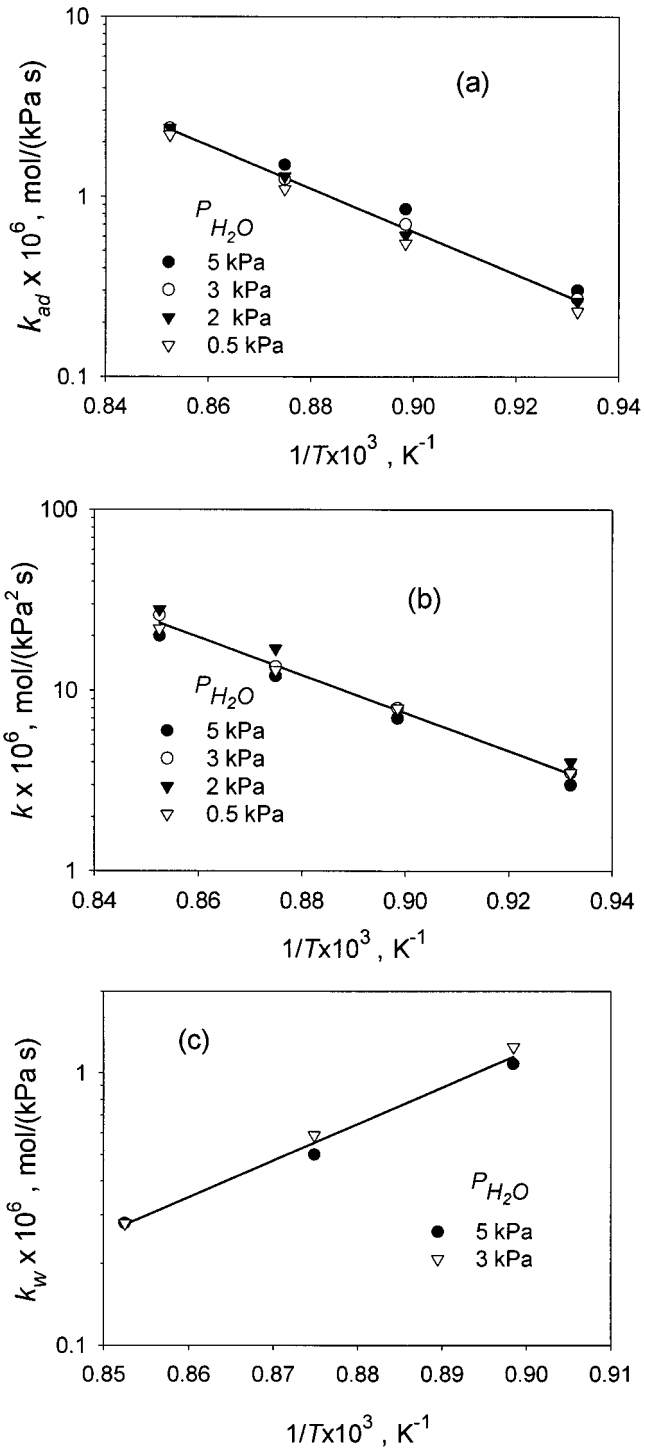

Figure 9. Temperature dependence (a) of the kinetic constant for CH_4 dissociative adsorption, k_{ad}, and of the apparent kinetic constants (b) k (eq 14) and (c) k_w (eq 19) at various P_{H_2O} values. The solid lines correspond to the values of the kinetic constants and activation energies in Table 1.

Table 1. Mean Values of the Parameters k_{ad}, k, k_w, E_a, E, and E_w Used in the Kinetic Model (Eqs 8, 13, and 18), As Determined by Fitting the Kinetic Model to the Experimental Data

T, K	k_{ad}, mol/(kPa s)	k, mol/(kPa^2 s)	k_w, mol/(kPa s)	E_{ad}, kcal/mol	E, kcal/mol	E_w, kcal/mol
1073	0.26×10^{-6}	3.44×10^{-6}				
1113	0.66×10^{-6}	7.75×10^{-6}	1.03×10^{-6}			
1143	1.26×10^{-6}	1.37×10^{-5}	0.55×10^{-6}	54.7 ± 2.2	48.1 ± 2.1	-61.6 ± 3.4
1173	2.33×10^{-6}	2.35×10^{-5}	0.27×10^{-6}			

as high as 61 kcal/mol at temperatures between 1073 and 1173 K.

Because of the rate-determining character of the surface reaction represented by eq 9, the apparent activation energy is strongly affected upon variation of the gas-phase composition, thus decreasing with increasing P_{CH_4}/P_{H_2O} ratio (Figure 8). This supports the view that the significant variation of the activation energies reported in the literature can be partly attributed to the fact that different gas compositions were used in the corresponding studies.

Kinetic Behavior. In the present study, the reaction rate was found to exhibit zero-order kinetic behavior with respect to P_{H_2O}. This observation does not seem to be in agreement with previous kinetic studies of methane steam reforming on Ni−YSZ−cermet anodes, where negative reaction orders were observed.[3,5,6] However, both negative and positive as well as zero-order rate dependence have been reported by researchers who studied the kinetics of methane steam reforming reaction on supported Ni-based catalysts.[1,9−18] It was also observed that, under the same reaction conditions, the rate maximum location, with respect to P_{CH_4} appeared at significantly lower P_{CH_4} values.[5,7] The above discrepancies and contradictions are frequently observed in the literature, and it is likely that this behavior is due to the varying catalytic activity of the Ni catalysts toward the surface reactions leading to the conversion of methane to CO and H_2. Variations in catalytic activity can be attributed to problems related with the reproducibility of catalyst preparation and activation methods.[2] It is plausible that the Ni surface area, dispersion, and crystallite size play a dominant role in the activation of the surface reactions occurring on the Ni surface.

According to the above-proposed kinetic model, differentiation of eq 13 with respect to P_{CH_4} at the rate maximum location leads to the following relation for estimation of the $P_{CH_4,max}$ value at the rate maximum (the term $kP_{CH_4}^2 r_{CO_2}$ in eq 13 was neglected because it is 3 orders of magnitude smaller than $k_{ad}P_{CH_4}P_{H_2O}F_t$):

$$k = \frac{{k_{ad}}^2}{K_{H_2O}k_r} = \frac{F_t}{3}\frac{P_{H_2O}}{{P_{CH_4,max}}^2} \qquad (21)$$

Thus, it can be easily concluded (eq 21) that, with increasing k, the rate maximum is shifted toward lower P_{CH_4} values. Variation in the value of k can be caused either by variations in the Ni surface area, thus affecting proportionally k_{ad} and k_r, or by changes in k_{ad}, k_r, and K_{H_2O}, due to alterations in the electronic properties of the catalyst surface. The latter can be most probably attributed to changes in the crystallite size.

Carbon Formation. Bebelis et al.[7] measured rates of carbon formation with selectivities approaching 15%, while the reforming reaction rate maximum at 1100 K and $P_{H_2O} \cong 0.75$ kPa corresponded to $P_{CH_4} \cong 4$ kPa, which is 8 times lower than the value of 30 kPa observed in the present study. According to eq 21, this difference implies a significant increase in k_{ad} and a corresponding decrease in k_r. A large difference in the rates of the reaction steps of eqs 7 and 9 most likely favors carbon formation on the catalytic surface because the high coverages of active carbon may render the formation of graphitic carbon thermodynamically feasible. Duprez et al.,[28] who studied coke formation on Ni−Al_2O_3 catalysts, reported that the surface carbon nucleates into graphitic filaments, where about 8 carbon atoms correspond to each surface Ni atom. The addition of small quantities of Mo or Li was reported to lower the activation energy for oxidative removal of deposited carbon by about 50 kJ/mol,[29] most propably because of the induced electronic effect on the Ni surface. According to Besenbacher et al.,[27] who proposed the design of a Ni/Au surface alloy based on density functional theory calculations, the probability of graphite nucleation in the steam reforming reaction is essentially determined by the coverage of active C_{ad}. This coverage depends on the stability of the adsorbed carbon atoms, C_{ad}, i.e., the less stable the adsorbed C_{ad}, the larger the tendency to react with adsorbed O_{ad} (higher k_r) to form CO. Thus, a robust steam reforming catalyst should be characterized by high catalytic activity toward the surface reaction described by eq 9, as compared to the activation of CH_4 adsorption (eq 7).

Effect of Anodic Polarization. Concerning the effect of anodic polarization on carbon formation, Bebelis et al.[7] have shown that the rate of carbon deposition on a Ni−YSZ−cermet anode is reduced by 33% upon positive polarization of the anode, which shows the positive effect of the applied current and potential on the kinetics of CH_4 transformation toward CO, CO_2, C, and H_2. Although no kinetic experiments were carried out in the present study under closed-circuit conditions, there is experimental evidence[5] that the O^{2-} supply to the Ni−YSZ−cermet anode will also result in electrochemical transformation of CH_4 either toward CO and H_2 or toward CO_2 and H_2O, depending on the P_{CH_4}/P_{H_2O} ratio, inhibiting carbon deposition onto the surface of the anodic electrode. However, the kinetic behavior of the catalytic steam reforming reaction is not expected to be significantly affected under fuel cell operation conditions, concerning its general features and the functional form of the kinetic model equations.

Conclusions

The kinetics of the steam reforming of methane on Ni−YSZ−cermet films deposited on a YSZ disk involve two rate-limiting steps, which are represented by the activated adsorption of CH_4 for the production of active species (most probably in the form of active C_{ad}) and the surface reaction of the adsorbed C_{ad} with O_{ad} (originating from water dissociative adsorption) for the production of CO. The relative magnitude of the turnover frequencies of these two rate-limiting steps affects considerably the apparent activation energy of the reaction at different P_{CH_4} and P_{H_2O} values as well as the tendency of the reaction system to generate graphitic carbon on the catalytic surface. A catalytic surface

resistive to carbon deposition will rather promote the surface reaction of active carbon with O_{ad} than the activation of CH_4 adsorption.

Acknowledgment

Financial support by the PENED Program of the Hellenic General Secretariat of Research and Technology is gratefully acknowledged.

Literature Cited

(1) Rostrup, J. R.-N. Steam reforming. In *Catalysis—Science and Technology*; Anderson, J. R., Boudart, M., Eds.; Springer-Verlag: Berlin, 1983; Vol. 5.

(2) Zanibelli, L.; Flego, C.; Perego, C.; Rizzo, C. A Catalytic study of Ni/YSZ cermets for internal reforming SOFC. In *Proceedings of the 1st European SOFC Forum*, Lucerne, Switzerland, 1994; Bossel, U., Ed.; European SOFC Forum: Baden, Switzerland, Vol. 1, p 207.

(3) Lee, A. L.; Zabransky, R. F.; Huber, W. J. Internal Reforming Development for Solid Oxide Fuel Cells. *Ind. Eng. Chem. Res.* **1990**, *29*, 766.

(4) Belyaev, V. D.; Politova, T. I.; Mar'ina, O. A.; Sobyanin, V. A. Internal steam reforming of methane over Ni-based electrode in solid oxide fuel cells. *Appl. Catal.* **1995**, *133*, 47.

(5) Yentekakis, I. V.; Jiang, Y.; Neophytides, S.; Bebelis, S.; Vayenas, C. G. Catalysis, electrocatalysis and electrochemical promotion of the steam reforming of methane over Ni film and Ni—YSZ cermet anodes. *Ionics* **1995**, *1*, 491.

(6) Dicks, A. L.; Pointon, K. D.; Siddle, A. Intrinsic reaction kinetics of methane steam reforming on a nickel/zirconia anode. *J. Power Sources* **2000**, *86*, 523.

(7) Bebelis, S.; Neophytides, S.; Vayenas, C. G. Kinetic and electrokinetic behaviour of the Ni—YSZ cermet electrodes for the methane steam reforming reaction: Effect of electrode potential. In *Proceedings of the 1st European SOFC Forum*, Lucerne, Switzerland, 1994; Bossel, U., Ed.; European SOFC Forum: Baden, Switzerland, Vol. 1, p 197.

(8) Yentekakis, I. V.; Neophytides, S. G.; Kaloyannis, A. C.; Vayenas, C. G. Kinetics of internal steam reforming of methane and their effect on SOFC performance. In *Proceedings of the 3rd International Symposium on SOFCs*; Singhal, S. C., Iwahara, H. Eds.; The Electrochemical Society: Pennington, NJ, 1993, PV 93-4, p 904.

(9) Akers, W. W.; Camp, D. P. Kinetics of the methane steam reaction. *AIChE J.* **1955**, *1*, 471.

(10) Atrochenko, V. I.; Raman, S. K.; Zryagintsev, G. I. Kinetics of conversion of natural gas by steam under pressure. *J. Appl. Chem. USSR* **1969**, *42*, 1496.

(11) Bodrov, N. M.; Apel'baum, L. O.; Temkin, M. I. The kinetics of the reaction between methane and water vapor on a Ni surface at 400—600 °C. *Kinet. Katal.* **1967**, *8*, 821.

(12) Ross, J. R. H.; Steel, M. C. F. Mechanism of the steam reforming of methane over a precipitated nickel—alumina catalysts. *J. Chem. Soc., Faraday Trans.* **1972**, *1*, 69.

(13) Quach, P. T.; Rouleau, U. D. Kinetics of the steam reforming reaction over Ni catalyst in CSTR reactor. *J. Appl. Chem. Biotechnol.* **1975**, *25*, 459.

(14) Munster, P.; Grabke, H. J. Kinetics of the steam reforming of methane with iron, nickel, and iron—nickel alloys as catalysts. *J. Catal.* **1981**, *72*, 279.

(15) De Deken, J. C.; Devosm, E. F.; Froment, G. F. Steam reforming of natural gas: intrinsic kinetics, diffusional influences and reactor design. *ACS Symp. Ser.* **1982**, 196.

(16) Xu, J.; Froment, G. F. Methane steam reforming, methanation and water—gas shift: I. Intrinsic kinetics. *AIChE J.* **1989**, *35* (1), 88.

(17) Elnashaie, S. S. E.; Adris, A. M.; Al-Ubaid, A. S.; Soliman, M. A. On the non-monotonic behaviour of methane—steam reforming kinetics. *Chem. Eng. Sci.* **1990**, *45* (2), 491.

(18) Castro Luna, A. E.; Becerra, A. M. Kinetics of methane steam reforming on a Ni on alumina—titania catalyst. *React. Kinet. Catal. Lett.* **1997**, *61* (2), 369.

(19) Sotiropoulou, D.; Ladas, S. An XPS and XAES study of the Ni/ZrO_2 interface. *Surf. Sci.* **1998**, *408*, 182.

(20) Bradford, M. C. J.; Vannice, M. A. CO_2 reforming of CH_4. *Catal. Rev.—Sci. Eng.* **1999**, *41* (1), 1.

(21) Beebe, T. P., Jr.; Goodman, D. W.; Kay, B. D.; Yates, J. T., Jr. Kinetics of the activated dissociative adsorption on the low index planes of nickel single-crystal surfaces. *J. Chem. Phys.* **1987**, *87* (4), 2305.

(22) Lee, M. B.; Yang, Q. Y.; Ceyer, S. T. Dynamics of the activated dissociative chemisorption of CH_4 and implication for the pressure gap in catalysis: A molecular beam-high-resolution electron energy loss study. *J. Chem. Phys.* **1987**, *87* (5), 2724.

(23) Avdeev, V. I.; Zhidomirov, G. M. Theoretical Analysis of Methane Decomposition at the Ni(100) Surface. *Kinet. Catal.* **1994**, *35* (2), 225—231.

(24) Holmblad, P. M.; Wambach, J.; Chorkendorf, I. Molecular beam study of dissociative sticking of methane on Ni(100). *J. Chem. Phys.* **1995**, *102* (20), 8255.

(25) Wu, M. C.; Goodman, D. W. High-resolution electron energy-loss measurements of sticking coefficients of methane decomposition on Ru(0001). *Surf. Sci. Lett.* **1994**, *306*, L529.

(26) Kratzer, P.; Hammer, B.; Nørskov, J. K. A theoretical study of CH_4 dissociation on pure and gold-alloyed Ni(111) surfaces. *J. Chem. Phys.* **1996**, *105* (13), 5595.

(27) Besenbacher, F.; Chorkendoff, I.; Clausen, B. S.; Hammer, B.; Molenbroek, J. K.; Nørskov, A. M.; Stensgaard, I. Design of a surface alloy catalyst for steam reforming. *Science* **1998**, *279*, 1913.

(28) Duprez, D.; Demicheli, M. C.; Marceot, P.; Barbier, J.; Ferreti, O. A.; Ponzi, E. N. Deactivation of steam reforming Model Catalysts by coke formation. *J. Catal.* **1990**, *124*, 324.

(29) Coe, N. J.; Cunningham, R. H.; Ormerod, R. M. Calculation of metal—carbon bond strength of surface carbon deposited on solid oxide fuel cell nickel/zirconia fuel reforming anodes. *Catal. Lett.* **1997**, *49*, 189

Received for review March 30, 2000
Revised manuscript received August 10, 2000
Accepted August 16, 2000

IE000350U